# $K$-shell x-ray production cross sections for $^{12}C$, $^{14}N$, and $^{16}O$ ions on Ni, Rb, Ag, and Sb: 0.4–2.4 MeV/amu*

Tom J. Gray,† Patrick Richard, and Robert L. Kauffman‡
*Physics Department, Kansas State University, Manhattan, Kansas 66506*

T. C. Holloway, R. K. Gardner, G. M. Light, and J. Guertin
*Physics Department, North Texas State University, Denton, Texas 76201*

(Received 19 November 1975)

$K$-shell x-ray production cross sections for $^{12}C$, $^{14}N$, and $^{16}O$ ions on thin targets of Ni, Rb, Ag, and Sb were measured over the incident-ion energy range of 0.4–2.4 MeV/amu. Comparisons to theoretical predictions of the binary-encounter, semiclassical, and plane-wave Born approximations (PWBA) show that these theories overpredict the magnitude of the measured cross sections. The PWBA calculations with perturbation corrections for binding energy and Coulomb deflection effects included are in better agreement with the measured data for $E/M < 1.2$ MeV/amu. Comparison of the data to the perturbed PWBA calculations which also include corrections of electron polarization effects in the case of $^{12}C$ on Ni gives good agreement between these theoretical estimates and the measured $K$-shell x-ray production cross sections.

## I. INTRODUCTION

Theoretical investigations of the inner-shell ionization process for light ions have developed along semiclassical and quantum-mechanical approaches as represented by the binary-encounter approximation (BEA) by Garcia and co-workers,[1] the constrained binary-encounter approximation (CBEA) by Hansen,[2] the semiclassical approximation (SCA) by Hansteen and Mosebeck,[3] and the plane-wave Born approximation (PWBA) by Khandelwahl, Choi, and Merzbacher.[4] Inherent in each of these theories is the requirement that the ratio of the projectile charge ($Z_1$) and target atomic number ($Z_2$) have the property that $Z_1/Z_2 \ll 1$. Recent work by several research groups[5] has shown for $K$-shell ionization by proton impact that the description for the observed x-ray or ionization cross sections may be represented equivalently by the above theories. The agreement between the experimental cross-section data for proton impact and the theoretical estimates is generally quite good over an energy range of <0.5 to ~5 MeV/amu.

In the cases of $^4He$ bombardment,[6] $^6Li$ bombardment,[7] and $^7Li$ bombardment[8] the PWBA, BEA, and SCA theoretical predictions for the $K$-shell x-ray production cross sections for elements with $Z_2 \geq 22$ have the common characteristic of overpredicting the measured cross sections by increasingly larger amounts as $Z_1$ is increased from $Z_1 = 2$(He) to $Z_1 = 3$(Li).

The inclusion of perturbation effects for the ion-nucleus interaction (Coulomb deflection effect) and the change in the effective electron binding energy during the passage of the projectile (binding energy effect) reported by Basbas, Brandt, and Laubert[9] as corrections to the PWBA calculations lower the magnitude of the calculated cross sections to give much better agreement with the observed x-ray cross-section data over a wide range of target atomic numbers. These perturbation effects introduce $Z_1/Z_2$ dependences into the calculated cross sections which cause increasingly strong deviations from the $Z_1^2$ dependence common to the BEA, CBEA, SCA, and PWBA theories. The perturbation effects for proton impact have not proven to be that effective, because of the relatively small magnitude of the corrections except at the lower energies ($E \lesssim 0.5$ MeV/amu), where the Coulomb deflection correction increases rather strongly because of the large increases in the Rutherford-scattering cross sections.

The present work was initiated to measure the $K$-shell x-ray production cross section for the heavier ions, $^{12}C$, $^{14}N$, and $^{16}O$, on the elements Ni, Rb, Ag, and Sb. The measurements of the x-ray cross sections were made during a single accelerator run with a fixed experimental geometry to minimize problems often encountered in data normalization procedures. The range of targets studied and projectile energies investigated were chosen to provide a systematic picture of the inner-shell ionization process for incident ions on targets where $Z_1/Z_2$ ranged from $Z_1/Z_2 < 0.29$ to $Z_1/Z_2 \ll 1$. Comparisons of the data to theoretical predictions are given for the BEA, SCA, PWBA, and PWBA with Coulomb deflection and binding energy corrections (PWBABC). In the case of $^{12}C$ on Ni corrections for the polarization effect are also included in the theoretical calculations.

## II. EXPERIMENTAL PROCEDURE

Thin targets of Cu, RbCl, Ag, and Sb were prepared by evaporating the desired material onto thin carbon backings by standard evaporation techniques. The target thicknesses were found to be 12 $\mu g/cm^2$ (Ni), 33 $\mu g/cm^2$ (Rb component of $RbCl_3$), 38 $\mu g/cm^2$ (Ag), and 50 $\mu g/cm^2$ (Sb) by measuring elastic proton scattering at an energy of 1.50 MeV and a laboratory angle of 150° using the 2.5-Mv Van de Graaff accelerator at North Texas State University. The targets were placed at a 60° angle to the incident beam. The x rays were detected at 90° to the beam direction and elastically scattered particles were measured at laboratory angles of 30°, 45°, 135°, or 150° depending upon kinematical and energy-loss criteria. The x-ray energy spectra and charged-particle-scattering spectra were recorded simultaneously to allow data reduction by normalization to the Rutherford-scattering cross section. This technique has been discussed previously.[10] For the majority of the present work the 30° and 45° detectors were utilized to measure the charged particle scattering to assure that the nuclear scattering was Rutherford in character. As reported previously,[8] care must be exercised to account for deviations arising from nuclear contributions to the elastic scattering.

The x-ray detector efficiency and solid angle were determined using standardized x-ray sources as reported previously.[10] The x rays were brought out of the target chamber through a 0.13-mm Mylar vacuum window and passed through a 0.38-mm Mylar absorber before entering the 3-mm $\times 30$-$mm^2$ Kevex Si(Li) x-ray detector. The absorber was utilized to decrease the large $L$-shell x-ray components encountered for the Ag and Sb targets. The x-ray detector had a resolution of 180 eV at 5.895 keV. The x-ray count rate was limited to less than 200 counts per second in order to minimize dead-time corrections. A 2-$\mu$sec time constant was used in the x-ray detector preamplifier-amplifier system and the dead time, live time, and true time were recorded in all cases to allow proper corrections to be applied where necessary.

Ion beams of $^{12}C$, $^{14}N$, and $^{16}O$ were obtained using the model EN tandem Van de Graaff accelerator at the Kansas State University laboratory. The incident beam charge states ranged from 3+ to 5+ depending upon the ion energy. The targets used in this work were sufficiently thick to ensure that charge state equilibrium was attained within the target. No charge state effects were observed for the present set of measurements. The beam energies ranged from 0.4 to 2.4 MeV/amu, with energy steps of 0.2 MeV/amu.

## III. DATA ANALYSIS

The x-ray production cross sections were determined from the relationship

$$\sigma_{KX}(E_1) = T\left(\frac{Y_{K\alpha}}{\epsilon_{K\alpha}} + \frac{Y_{K\beta}}{\epsilon_{K\beta}}\right)\frac{\sigma_R(E_1)}{Y_R(E_1)}\,d\Omega\,,$$

where $Y_{K\alpha}$ and $Y_{K\beta}$ are the measured $K\alpha$ and $K\beta$ x-ray yields, $\epsilon_{K\alpha}$ and $\epsilon_{K\beta}$ are the x-ray detector efficiencies at the respective $K\alpha$ and $K\beta$ x-ray energies, $Y_R(E_1)$ is the measured nuclear elastic scattering at laboratory angle $\theta$, $d\Omega$ is the charged particle solid angle, $T$ is the dead-time correction factor, and $\sigma_R(E_1)$ is the Rutherford-scattering cross section at beam energy $E_1$. The ratios of $K\alpha$ and $K\beta$ yields were determined and corrected for the relative efficiencies of the x-ray detector. Table I gives the measured x-ray production cross sections and $K\alpha/K\beta$ ratios for the incident ions employed in this work.

Error analysis of the data includes contributions from statistical uncertainties of $\lesssim 3\%$ for $Y_{K\alpha}$, $\lesssim 5\%$ for $Y_{K\beta}$, and $\lesssim 2\%$ for $Y_R$, with combined uncertainties in calibration source strength, source x-ray yields, and relative photon intensities of $<5\%$. The relative uncertainty in the measured cross sections is $<6\%$, while the absolute normalization uncertainty is taken as being $<9\%$. The errors associated with the $K\alpha/K\beta$ ratios are taken as being $<15\%$. The errors in the target thickness measurements are $\lesssim 5\%$.

## IV. RESULTS AND DISCUSSION

Shown in Fig. 1 is a comparison of the experimental $K$-shell x-ray production cross sections for $^{12}C$ on Ni from this work and predictions of the PWBA, PWBABC, BEA, and SCA. The values of fluorescence yields $\omega_K$ used in calculating the theoretical x-ray production cross sections were taken from the theoretical predictions of McGuire.[11] The use of single-hole values for the radiation parameters is an assumption based upon estimates of the effects of multiple ionization on $\omega_K$ using the scaling technique of Larkins.[12] The values of $\omega_K$ calculated for the defect configuration up to $(1s)^{-1}(2p)^{-5}$ are given in Table II for Ni and Ag.

The fluorescence yield is estimated to change by a maximum of 16% for the $(1s)^{-1}(2p)^{-5}$ configuration in Ni. Computation of an effective value for $\omega_K$ to account for the multiple-ionization effects in the x-ray cross section yields changes which are of the same order of correction as the errors in the measured data. In view of the magnitudes of the data and theoretical estimates, single-hole values of $\omega_K$ were used in comparisons between the data and the theoretical predictions. Kauffman *et al.*[13] have measured the $K\alpha$ satellite intensities

TABLE I. $K$-shell x-ray production cross sections and $K\alpha/K\beta$ ratios.

| Element \ Incident ion | $E/M$ | $^{12}C$ $\sigma_x$ (b) | $^{12}C$ $K\alpha/K\beta$ | $^{14}N$ $\sigma_x$ (b) | $^{14}N$ $K\alpha/K\beta$ | $^{16}O$ $\sigma_x$ (b) | $^{16}O$ $K\alpha/K\beta$ |
|---|---|---|---|---|---|---|---|
| $_{28}Ni$ | 0.4 | 2.98 | 7.18 | 2.79 | 7.85 | 2.59 | 7.53 |
| | 0.6 | 12.7 | 7.36 | 12.8 | 7.85 | 12.4 | 7.01 |
| | 0.8 | 33.9 | 6.96 | 35.9 | 6.55 | 37.3 | 6.53 |
| | 1.0 | 86.9 | 6.39 | 90.3 | 6.29 | 86.0 | 6.30 |
| | 1.2 | 172 | 6.35 | 182 | 5.98 | 192 | 5.90 |
| | 1.4 | 301 | 5.70 | 325 | 5.95 | 380 | 5.70 |
| | 1.6 | 610 | 5.84 | 571 | 6.08 | 709 | 5.49 |
| | 1.8 | 945 | 5.83 | 939 | 5.67 | 1080 | 5.43 |
| | 2.0 | 1350 | 5.86 | 1420 | 5.59 | 1590 | 5.42 |
| | 2.2 | 1760 | 5.89 | 2020 | 5.60 | 2500 | 5.45 |
| | 2.4 | | | | | 3310 | 5.45 |
| $_{37}Rb$ | 0.4 | 0.174 | 5.64 | | | 0.157 | 6.48 |
| | 0.6 | 1.10 | 5.45 | 1.01 | 6.35 | 0.986 | 5.98 |
| | 0.8 | 2.92 | 6.16 | 3.07 | 5.59 | 3.14 | 5.94 |
| | 1.0 | 6.32 | 5.99 | 7.17 | 6.08 | 7.03 | 5.86 |
| | 1.2 | 12.6 | 5.72 | 14.0 | 5.99 | 14.0 | 5.58 |
| | 1.4 | 21.2 | 5.66 | 22.9 | 5.78 | 25.6 | 5.33 |
| | 1.6 | 35.8 | 5.90 | 37.3 | 5.72 | 41.4 | 5.05 |
| | 1.8 | 56.2 | 5.87 | 57.2 | 5.07 | 61.8 | 5.14 |
| | 2.0 | 84.2 | 5.25 | 88.2 | 5.28 | 95.5 | 5.04 |
| | 2.2 | 118 | 5.17 | 125 | 5.08 | 134 | 4.89 |
| | 2.4 | | | 162 | 5.09 | 186 | 4.83 |
| $_{47}Ag$ | 0.4 | 0.0161 | 4.28 | | | 0.0151 | 4.17 |
| | 0.6 | 0.127 | 4.92 | 0.166 | 2.89 | 0.146 | 4.31 |
| | 0.8 | 0.414 | 4.03 | 0.484 | 4.09 | 0.500 | 5.30 |
| | 1.0 | 1.03 | 4.11 | 1.03 | 5.33 | 1.16 | 5.03 |
| | 1.2 | 1.88 | 5.14 | 2.05 | 5.18 | 2.29 | 4.83 |
| | 1.4 | 3.19 | 4.68 | 3.32 | 6.05 | 4.17 | 4.76 |
| | 1.6 | 5.18 | 5.38 | 5.65 | 5.02 | 7.21 | 5.02 |
| | 1.8 | 8.29 | 4.51 | 8.93 | 4.22 | 9.49 | 3.95 |
| | 2.0 | 12.9 | 4.09 | 11.3 | 4.97 | 13.6 | 5.51 |
| | 2.2 | 16.5 | 4.63 | 16.2 | 5.22 | 18.8 | 4.03 |
| | 2.4 | | | 21.2 | 4.59 | 22.8 | 4.13 |
| $_{51}Sb$ | 0.4 | | | | | | |
| | 0.6 | | | | | 0.0536 | 6.22 |
| | 0.8 | 0.176 | 3.28 | 0.230 | 3.37 | 0.214 | 4.13 |
| | 1.0 | 0.412 | 5.77 | 0.510 | 3.68 | 0.515 | 4.40 |
| | 1.2 | 0.856 | 5.24 | 0.916 | 4.38 | 0.991 | 4.48 |
| | 1.4 | 1.40 | 4.29 | 1.59 | 4.28 | 1.73 | 4.56 |
| | 1.6 | 2.40 | 4.01 | 2.45 | 4.08 | 2.97 | 4.83 |
| | 1.8 | 3.86 | 3.46 | 4.06 | 3.31 | 4.43 | 3.70 |
| | 2.0 | 5.18 | 4.25 | 5.12 | 4.21 | 6.03 | 3.64 |
| | 2.2 | 6.43 | 4.01 | 8.01 | 3.52 | 8.33 | 3.58 |
| | 2.4 | | | 8.43 | 4.57 | 10.78 | 3.69 |

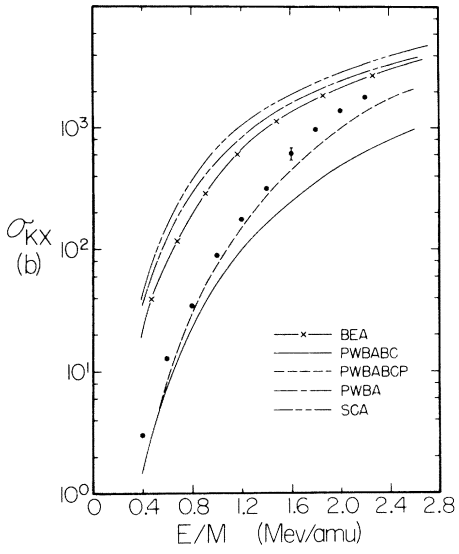


FIG. 1. $K$-shell x-ray production cross section for $^{12}C$ ions on a thin Ni ($Z=28$) target. The corrected plane-wave Born approximation calculations (PWBABC) were taken from Ref. 9. The inclusion of the high-velocity polarization effects is based upon calculated cross sections supplied by G. Basbas (Ref. 16). The theoretical cross sections were calculated using single-hole values for $\omega_K$. The theoretical x-ray production cross sections are estimated to increase by ~16% for $^{12}C$ on Ni when Larkin's values of $\omega_K$ (Ref. 12) are used in lieu of the single-hole values of $\omega_K$. B, C, and P refer to the binding energy, Coulomb deflection, and polarization corrections, respectively, taken from Ref. 9 and Ref. 15.

for 30-MeV oxygen on targets of Cu through Mn for which the most probable hole configuration varies from $KL_3$ to $KL_2$, respectively. Chaturvedi *et al.*[14] have reported energy shift measurements for $^{16}O$ ions at ~1.5 MeV/amu on Ti, Co, and Ge $K\alpha$ and $K\beta$ x-ray lines which suggest a most probable hole configuration of ~$KL_2$ at ~2.0 MeV/amu. Similar results for $^{12}C$ on these elements[14] at ~2.0 MeV/amu suggest the same type of vacancy configuration for the $K$-shell. It is reasonable to expect $^{14}N$ bombardment to yield similar results. This assumption is strengthened in view of the similarity of the $K\alpha/K\beta$ ratios given in Table I. The agreement in the magnitude of these ratios and their similar dependence on incident ion energy for $^{12}C$, $^{14}N$, and $^{16}O$, within the assigned error, suggest that the behavior of the multiple-ionization effects is essentially equivalent for the heavy-ion–target combinations in the present work. The assumption that single-hole values for $\omega_K$ may be representative of the radiative parameters can be replaced when further developments in theory or experiment provide more adequate descriptions of fluorescence yields for systems such as those reported in the present work.

TABLE II. Scaled values for $\omega_K$ assuming defect configurations of $(1s)^{-1}(2p)^{-n}$.

| $n$ | $\omega_K$ Ni ($Z_2=28$) | $\omega_K$ Ag ($Z_2=47$) |
|---|---|---|
| 0 | 0.45 | 0.85 |
| 1 | 0.48 | 0.86 |
| 2 | 0.50 | 0.87 |
| 3 | 0.52 | 0.88 |
| 4 | 0.53 | 0.88 |
| 5 | 0.47 | 0.84 |

Because of the similarity of the previous data for energy shifts of the $K\alpha$ and $K\beta$ x rays under $^{16}O$ and $^{12}C$ bombardment[14,15] it is expected that the relative cross sections for $K$-shell x-ray production for $^{12}C$, $^{14}N$, and $^{16}O$ will be independent of major variations in $\omega_K$, to first order. Hence observations of the x-ray production cross sections for $^{12}C$, $^{14}N$, and $^{16}O$ should be indicative of the relative $K$-shell ionization cross sections for these incident ion species on targets such as Ni, Rb, Ag, and Sb.

With the use of $\omega_K$ values as discussed above the BEA, SCA, and PWBA theories overpredict the observed cross sections for the energy range of the present work. Above 1.2 MeV/amu the measured data begin to approach the cross-section values predicted by the uncorrected theories. This type of energy-dependent behavior associated with $K$-shell ionization has been previously reported for the lighter incident ion species $^7Li$ on Ni and other elements.[8] At the lower energies, i.e., $E/m<1.2$ MeV/amu, the data are in good agreement with the predictions of the PWBABC. Furthermore, comparisons are made to preliminary calculations for the $K$-shell x-ray production cross section which includes perturbation effects for high-velocity electron shell polarization by the incident ion.[16] This correction is included in addition to the Coulomb deflection and binding energy corrections and is denoted PWBABCP. The net effect of inner-shell polarization is to decrease the effective interaction distance between the incident ions and the electron through the distortion of the electron shell because of the nonadiabatic character of the ion-electron interaction at high velocity. This has the effect of decreasing the electron-target binding energy used in the unperturbed theoretical calculations for the ionization cross section. Inner-shell charge exchange interactions may also cause an enhancement in the x-ray production cross section. However, no comparisons have been made to calcu-

lated $K$-shell cross sections which include effects other than those normally associated with direct Coulomb ionization as found in the PWBA and corrected PWBABC theories.

The PWBABCP predictions are in good agreement with the measured $K$-shell x-ray production cross sections for $^{12}C$ on Ni. There is a problem with the PWBABCP calculations, however. For $E/m \lesssim 1.8$ MeV the values of the calculated cross section using the PWBABCP approach are determined using extrapolated reduced binding energy parameters $\theta_K$. The present tabulated values of the function $f(\theta_K, \eta_K)$, as found in the literature[4] for the PWBA calculations, are not of sufficient range in $\theta_K$ to allow calculations for the corrected PWBA cross sections from the tabulated functions. Without the corrections for $\theta_K$ as used in the PWBABC calculations, the originally tabulated functions $f(\theta_K, \eta_K)$ were sufficient for light-ion considerations. However, the replacement of $\theta_K$ by $\epsilon\theta_K$, where $\epsilon > 1$, causes the required values of $\epsilon\theta_K$ to fall off from the presently available tabulated function. Extrapolations of $\theta_K$ may introduce varying degrees of error into the calculations, de-

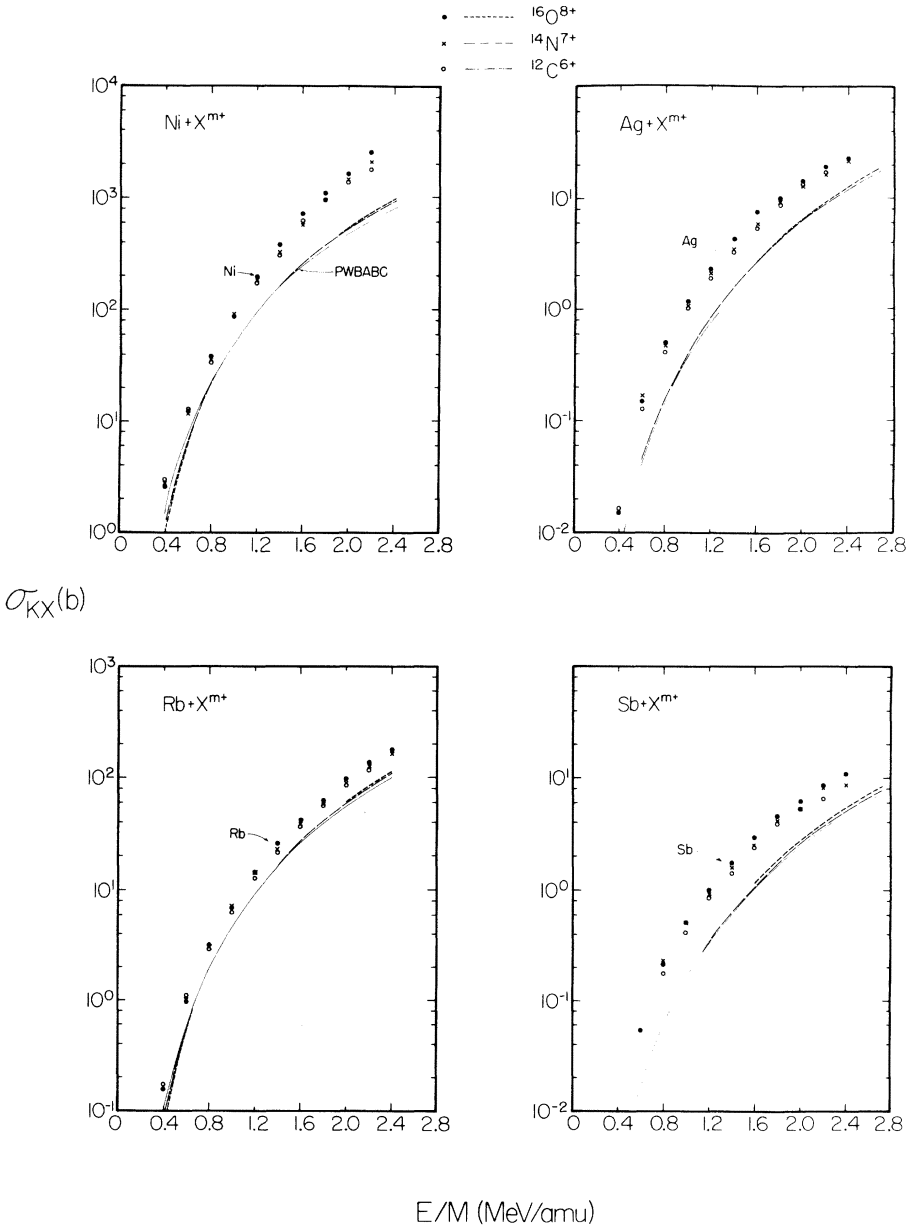


FIG. 2. $K$-shell x-ray production cross sections for $^{12}C$, $^{14}N$, and $^{16}O$ on Ni, Rb, Ag, and Sb.

TABLE III. Theoretical PWBA $K$-shell x-ray production with individual values for perturbations arising from consideration of the Coulomb deflection (CD) and binding energy (BE) corrections for 1.0-MeV/amu $^{12}C$, $^{14}N$, and $^{16}O$ on Ni with $\omega_K = 0.432$. Cross-section units are $10^{-24}$ cm$^2$.

| Ion | $^{12}C$ | $^{14}N$ | $^{16}O$ |
|---|---|---|---|
| PWBA | 517 | 704 | 919 |
| PWBA (CD) | 494 | 671 | 875 |
| PWBA (BE) | 54 | 53 | 50 |
| PWBABC | 52 | 50 | 47 |
| PWBA:PWBABC | 10:1 | 14:1 | 20:1 |

pending upon the functional behavior in the region of interest. In view of the extrapolation procedure for $E/M \lesssim 1.8$ MeV/amu it is suggested that the lower-energy regime of the PWBABCP predictions may represent a plausible behavior for the $K$-shell x-ray production cross section. The calculations approach the PWBABC calculations which were developed from the method of Ref. 9 using the formalism given in the work of Brandt and Lapicki.[17]

Shown in Fig. 2 are the x-ray production cross sections for $^{12}C$, $^{14}N$, and $^{16}O$ on Ni, Rb, Ag, and Sb over an energy range of ~0.4 to 2.4 MeV/amu. The measured cross sections do not scale by $Z_1^2$ as predicted by the unperturbed BEA, SCA, and PWBA theories. The PWBABC calculations are shown in Fig. 2 for comparison to the measured results for the cross sections. The general features of the calculated cross sections are in excellent agreement with the trends in the data. The relative magnitudes of the predicted $K$-shell x-ray production cross sections agree with the measurements. A crossover in the magnitude of the measured cross sections for the various projectiles is observed. This effect is predicted by the PWBABC theory. The relative contributions of the Coulomb deflection (CD) and binding energy (BE) corrections to the lowering of the calculated x-ray cross sections, when applied individually in the PWBA calculations, are given in Table III for 1.0-MeV/amu $^{12}C$, $^{14}N$, and $^{16}O$ ions on Ni. The BE correction is directly responsible for the majority of the decrease in the magnitude of the calculated cross section. Because of the relatively strong dependence of the BE corrections on $Z_1$, this is to be expected. The reduction in the calculated PWBA cross section as exhibited by the PWBABC predictions is a factor of 2 larger for $^{16}O$ than for $^{12}C$ in the case given in Table III. The observation of the underprediction of the absolute cross-section magnitude by the PWBABC is typical and has been observed for $^4He$ and $^7Li$ ions,[6,8] where questions associated with the use of single-hole values

TABLE IV. Experimentally measured ratios,[a] $R = Z_1'^2 \sigma_{KX}(Z_1)/Z_1^2 \sigma_{KX}(Z_1')$.

| Element | $E/M$ | ($^{14}N$, $^{12}C$)[b] $R_{expt.}$ | ($^{14}N$, $^{12}C$)[b] $R_{theor.}$ | ($^{16}O$, $^{12}C$) $R_{expt.}$ | ($^{16}O$, $^{12}C$) $R_{theor.}$ |
|---|---|---|---|---|---|
| $_{28}$Ni | 0.4 | 0.69 | 0.65 | 0.49 | 0.56 |
| | 0.6 | 0.74 | 0.67 | 0.55 | 0.60 |
| | 0.8 | 0.78 | 0.69 | 0.62 | 0.64 |
| | 1.0 | 0.76 | 0.71 | 0.56 | 0.67 |
| | 1.2 | 0.78 | 0.73 | 0.63 | 0.70 |
| | 1.4 | 0.79 | 0.74 | 0.71 | 0.72 |
| | 1.6 | 0.69 | 0.75 | 0.65 | 0.75 |
| | 1.8 | 0.73 | 0.77 | 0.64 | 0.77 |
| | 2.0 | 0.78 | 0.78 | 0.66 | 0.79 |
| | 2.2 | 0.84 | 0.79 | 0.80 | 0.81 |
| $_{37}$Rb | 0.4 | | | 0.51 | 0.47 |
| | 0.6 | 0.68 | 0.70 | 0.50 | 0.50 |
| | 0.8 | 0.77 | 0.72 | 0.61 | 0.52 |
| | 1.0 | 0.83 | 0.73 | 0.63 | 0.53 |
| | 1.2 | 0.82 | 0.74 | 0.77 | 0.55 |
| | 1.4 | 0.79 | 0.75 | 0.68 | 0.56 |
| | 1.6 | 0.77 | 0.76 | 0.65 | 0.58 |
| | 1.8 | 0.75 | 0.77 | 0.62 | 0.59 |
| | 2.0 | 0.77 | 0.77 | 0.64 | 0.60 |
| | 2.2 | 0.78 | 0.78 | 0.64 | 0.62 |
| $_{47}$Ag | 0.4 | | | 0.53 | 0.51 |
| | 0.6 | 0.71 | 0.73 | 0.65 | 0.54 |
| | 0.8 | 0.86 | 0.74 | 0.68 | 0.56 |
| | 1.0 | 0.74 | 0.75 | 0.63 | 0.57 |
| | 1.2 | 0.80 | 0.76 | 0.69 | 0.58 |
| | 1.4 | 0.77 | 0.76 | 0.74 | 0.59 |
| | 1.6 | 0.80 | 0.77 | 0.78 | 0.60 |
| | 1.8 | 0.79 | 0.78 | 0.64 | 0.61 |
| | 2.0 | 0.64 | 0.78 | 0.59 | 0.62 |
| | 2.2 | 0.72 | 0.79 | 0.64 | 0.63 |
| $_{51}$Sb | 0.8 | 0.96 | 0.75 | 0.68 | 0.57 |
| | 1.0 | 0.91 | 0.76 | 0.70 | 0.58 |
| | 1.2 | 0.79 | 0.77 | 0.65 | 0.59 |
| | 1.4 | 0.83 | 0.77 | 0.70 | 0.60 |
| | 1.6 | 0.75 | 0.78 | 0.70 | 0.61 |
| | 1.8 | 0.77 | 0.78 | 0.65 | 0.62 |
| | 2.0 | 0.73 | 0.79 | 0.66 | 0.63 |
| | 2.2 | 0.92 | 0.80 | 0.73 | 0.64 |

[a] Experimental errors are ≲15%.

[b] Notation ($^{14}N$, $^{12}C$) signifies $R = 36\sigma_{KX}(^{14}N)/49\sigma_{KX}(^{12}C)$.

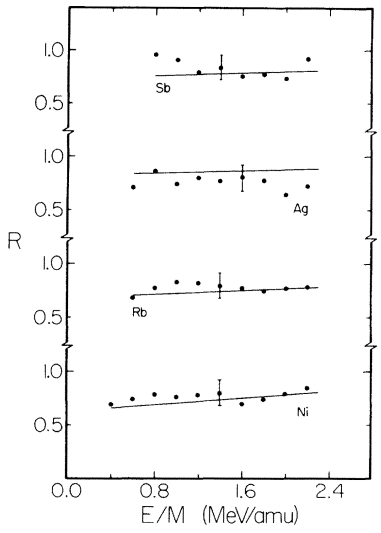


FIG. 3. Ratio $R = Z_1'^2\sigma_{KX}(Z_1)/Z_1^2\sigma_{KX}(Z_1')$ for $^{12}C$ and $^{14}N$ on Ni, Rb, Ag, and Sb. The unperturbed theories (PWBA, SCA, and BEA) predict $R = 1$ as the cross sections scale as $Z_1^2$. The ratio shown is for ($^{14}N$, $^{12}C$) as defined in Table IV.

of $\omega_K$ are minimized.

By taking the ratios of the experimental cross-section data for the different ion species at equivalent values of $E/M$ the experimental uncertainties in the system efficiency and $\omega_K$ cancel out. Therefore the ratio $R(Z_1, Z_1')$ defined as

$$R = Z_1'^2\sigma_{KX}(Z_1)/Z_1^2\sigma_{KX}(Z_1') ,$$

where $\sigma_{KX}(Z_1)$ and $\sigma_{KX}(Z_1')$ are the experimental (or theoretical) $K$-shell x-ray production cross sections, yields a direct comparison to the relative ionization cross sections. Given in Table IV are the experimental and theoretical (PWBABC) values for $R(^{14}N, ^{12}C)$ and $R(^{16}O, ^{12}C)$. Shown in Fig. 3 are the values of $R(Z_1, Z_1')$. The magnitude and energy-dependence differences between the measured and theoretical cross sections which are presented in Fig. 2 tend to cancel out of the values of $R(Z_1, Z_1')$ seen in Fig. 3. This is indicative of the similarity, even in the relative disagreement, between the PWBABC predictions and the data for the energy range and target-projectile combinations studied in this work. If viewed singularly, the values for $R(Z_1, Z_1')$ strongly support the PWBABC approach to calculating $K$-shell ionization cross sections. However, the disagreements between the measured and predicted cross-section magnitudes observed Fig. 2 suggest that further theoretical investigation be undertaken in order to better understand inner-shell ionization by fast heavy ions.

## V. CONCLUSIONS

This work has shown that the theory for $K$-shell ionization can be extended to the heavy-incident-ion species $^{12}C$, $^{14}N$, and $^{16}O$ in the range of targets $28 \lesssim Z_2 \lesssim 51$ if consideration for perturbation effects is included. The binding energy perturbation as found in the PWBABC approach is a major contributor to lowering the magnitudes of the calculated cross sections to give better agreement between the theory and experiment for the lower-energy portions of this work. The inclusion of the perturbation for the electron polarization effect does give a better overall agreement between the data and PWBABCP theory for $^{12}C$ on Ni. However, the extrapolation of $\theta_K$ used in the PWBABCP calculations for $E/M < 1.8$ needs to be replaced by a calculational technique of less uncertainty. Extension of the tabulated tables for the function $f(\theta_K, \eta_K)$ would be most helpful for future comparisons of theory and experiment in those cases where heavy ions are to be considered.

In order to properly compare the experimental data to the BEA and SCA theoretical predictions on the same basis as the PWBABC calculations it is suggested that further work be encouraged which may allow the inclusion of perturbation corrections for the binding energy effect to be included within the framework of the SCA and BEA theories for inner-shell ionization.

## ACKNOWLEDGMENT

We express our appreciation to G. Basbas for providing the PWBA calculations which included the corrections for the high-velocity polarization perturbation.

---

*Work supported in part by the Robert A. Welch Foundation, The Faculty Research Fund, North Texas State University, and the U. S. Energy Research and Development Administration under contract No. E(11-1)-2753.

†Presently on leave from North Texas State University.

‡Present address: Bell Laboratories, Murray Hill, N. J.

[1]J. D. Garcia, E. Gerjuoy, and J. E. Welker, Phys. Rev. 165, 66 (1968); J. D. Garcia, Phys. Rev. A 1, 1402 (1970); 1, 280 (1970).

[2]J. S. Hansen, Phys. Rev. A 8, 822 (1973).

[3]J. M. Hansteen and O. P. Mosebeck, Z. Phys. 234, 281 (1970).

[4]G. S. Khandelwal, B.-H. Choi, and E. Merzbacher, At. Data 1, 103 (1969).

[5]J. D. Garcia, R. J. Fortner, and T. M. Kavanagh, Rev. Mod. Phys. 45, 111 (1973).
[6]F. D. McDaniel, Tom J. Gray, and R. K. Gardner, Phys. Rev. A 11, 1607 (1975).
[7]F. Hopkins, R. Brenn, and A. R. Whitlemore, J. Karp, and S. K. Bhattacherjee, Phys. Rev. A 11, 916 (1975).
[8]F. D. McDaniel, Tom J. Gray, R. K. Gardner, G. M. Light, J. L. Duggan, H. A. Van Rinsvelt, R. D. Lear, G. H. Pepper, J. William Nelson, and Arlen R. Zander, Phys. Rev. A 12, 1271 (1975).
[9]G. Basbas, W. Brandt, and R. Laubert, Phys. Rev. A 7, 983 (1973).
[10]R. Lear and Tom J. Gray, Phys. Rev. A 8, 2469 (1973).
[11]E. J. McGuire, Phys. Rev. A 2, 273 (1970).
[12]F. D. Larkins, J. Phys. B 4, L29 (1971).
[13]R. L. Kauffman, J. H. McGuire, Patrick Richard, and C. F. Moore, Phys. Rev. A 8, 1233 (1973).
[14]R. P. Chaturvedi, J. L. Duggan, T. J. Gray, C. C. Sachtleben, and J. Lin, *Advances in X-ray Analysis*, Vol. 17, edited by C. L. Grant, C. S. Barrett, J. B. Newkirk, and C. O. Rudd (Plenum, New York, 1974), pp. 445 and 456.
[15]R. P. Chaturvedi, Tom J. Gray, G. Pepper, and J. L. Duggan, J. Tricomi, J. Lin, R. F. Carlton, E. L. Robinson, and P. D. Miller, Bull. Am. Phys. Soc. 19, 568 (1974).
[16]G. Basbas, private communication; W. Brandt, in *Proceedings of the International Conference on Inner Shell Ionization Phenomena and Future Applications, Atlanta, Georgia, 1972*, edited by R. W. Fink, S. T. Manson, J. M. Palms, and P. Venugopala Rao, CONF-720404 (Natl. Tech. Information Service, U. S. Dept. of Commerce, Springfield, Va., 1972), Vol. 2, p. 948.
[17]W. Brandt and G. Lapicki, Phys. Rev. A 10, 474 (1974).